A COMPARISON OF THEORY AND EXPERIMENT FOR COUPLED ROTOR-BODY STABILITY OF A HINGELESS ROTOR MODEL IN HOVER UNDER SIMULATED VACUUM CONDITIONS

William G. Bousman
Research Scientist
U.S. Army Aeroflightdynamics Directorate
Ames Research Center

Abstract

Two cases were selected for correlation from an experiment that examined the aeromechanical stability of a small-scale model rotor that used tantalum rods instead of blades to simulate vacuum conditions. The first case involved body roll freedom only while the second case included body pitch and roll degrees of freedom together. Analyses from Hughes Helicopters and the U.S. Army Aeromechanics Laboratory were compared with the data and the correlation ranged from poor to good.

Introduction

As a part of the Methodology Assessment two cases were selected from the experiments reported in Ref. 1 for comparison with theoretical models. Both cases selected were of a configuration that used tantalum rods instead of conventional blades to simulate vacuum conditions for the rotor. The body has only a roll degree of freedom for the first case, but both pitch and roll degrees of freedom for the second case. The use of tantalum rods instead of blades largely removes blade aerodynamic effects and it is therefore possible to judge the adequacy of structural and inertial modeling when theory and experiment are compared.

The theoretical models compared with the data included the Dynamic Analysis Research Tool (DART) and E927-1 analyses used by Hughes Helicopters and the FLAIR analysis developed at the U.S. Army Aeromechanics Laboratory. The other company codes were not used for this data set because of funding limitations.

The paper will briefly describe the experiment from which these data were obtained and then present the correlation. Conclusions will be made as to the quality of the agreement between theory and experiment. Appendices are provided that document the experimental model properties, tabulate the experimental data points, and show all of the correlations.

Experiment Description

The model used in this experiment is shown in Fig. 1. The rotor has three tantalum rods that act as blades mounted on flap and lead-lag flexures. The flexures are mounted to a hub supported by a static mast. The rotor, static mast, transmission, and two water-cooled electric motors are supported by ball bearings in a gimbal frame that allow body pitch and roll degrees of freedom.

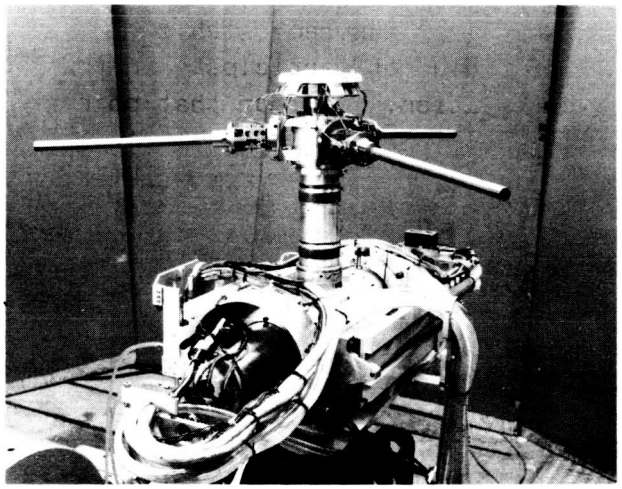

Fig. 1 Three-bladed rotor with tantalum rods mounted to gimbal with pitch and roll degrees of freedom.

The blade root flexures are shown in an exploded view in Fig. 2. Separate flap and lead-lag flexures contain essentially all of the flexibility of the rotor. The offset of both flexures is the same because of the folded-back load path. The major rotor properties are provided in Table 1.

Table 1 Tantalum Model Rotor Properties

Property	Value
Rotor radius, R, cm	38.01
Blade chord, c, cm	1.26
Solidity, σ	0.0318
Hinge offset, e/R	0.224
Lock number	0.0182

The effect of using tantalum rods of circular cross-section instead of conventional aerodynamic blades is that the lift curve slope is reduced to zero. Lock number is defined as

$$\gamma_d = \frac{\rho a c R^4}{I}\left(1 + \frac{c_{d_o}}{a}\right)$$

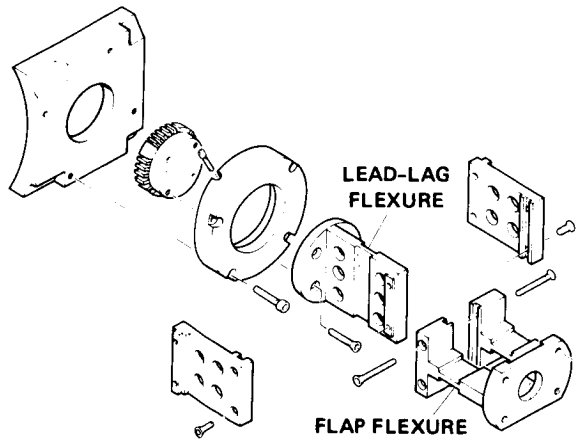

Fig. 2 Exploded view of blade root flexures.

where ρ is the density of air in g/cm^3, a is the lift curve slope, c the blade chord, R the rotor radius, I the blade flapping inertia, and c_{d_o} the blade profile drag coefficient. The term c_{d_o}/a is normally much less than 1 but as the lift curve slope approaches zero, the profile drag coefficient becomes important. To observe the rotor and body behavior for true vacuum conditions, it is necessary to reduce the density; however, this effect can be simulated by reducing the lift curve slope. For this experiment the use of tantalum rods reduced the Lock number to 0.2% of its value for conventional blades. This represents a good simulation of the vacuum condition, but the profile drag has been increased by two orders of magnitude. The mass properties of the tantalum rods were selected to match the blade nonrotating frequencies of the aerodynamic blades that were also tested in the experiment reported in Ref. 1. However, the hinge offset was effectively doubled, so rotating frequencies were not matched.

Damping and frequency data were obtained in this experiment by oscillating the rotor hub with a shaker at the modal frequency in the fixed system. When sufficient amplitude was achieved, the shaker was stopped and a pneumatic clamp on the shaker link was opened to release the model and allow the motions to freely decay. The damping and frequency were obtained using an analog equivalent of the moving-block analysis (Ref. 2). The lead-lag regressing-mode damping and frequency were measured in the fixed system following a transform to the multiblade coordinates and the quality of the data was quite good. However, body mode damping showed nonlinear behavior which was caused by Coulomb friction in the gimbal ball bearings (Ref. 3). A complete discussion of the model properties is provided as Appendix A. The experimental data used for correlation are provided in Appendix B.

Correlation

Two cases were used for correlation. These cases differed only in the body frequencies as shown in Table 2. For Case 1 the pitch degree of freedom was locked out, producing a pitch-mode frequency of 27 Hz which is well separated from the lead-lag regressing mode frequencies. Therefore, in the range of 0-10 Hz only one body mode is normally expected, but since there is no flap damping, both regressing lead-lag and flap modes should also be evident.

Table 2 Body Pitch and Roll Nonrotating Frequencies

Case	Body Pitch, Hz	Body Roll, Hz
1	27.0	2.56
2	2.58	2.55

Case 1

Modal frequency calculations are compared with the data in Fig. 3 for Case 1. The system behavior is seen most clearly by examining the predictions of the U.S. Army Aeromechanics Laboratory (Fig. 3c). The regressing lead-lag mode drops from its nonrotating value of 6.4 Hz and couples successively with the flap-progressing, body-roll, and flap-regressing modes before it reaches a zero frequency at about 500 rpm. The regressing lead-lag mode then increases in frequency and couples with the regressing flap mode, but within the test rotor speed range it does not coalesce with the body roll mode. For rotor speeds below 500 rpm the regressing lead-lag mode frequency is greater than 1/rev in the rotating system (stiff inplane), while above 500 rpm the frequency is less than 1/rev (soft inplane). It is in the latter case that rotors are susceptible to ground and air resonance.

For the Case 1 modal frequencies both the E927-1 and FLAIR codes show very good agreement with the measurements. Both codes match the data and reproduce the system behavior. However, the DART analysis shows only poor-to-fair correlation. Some reasons for this are understood and are worth discussing. The structural input for DART was derived from the tabulated mass and stiffness properties of Appendix A. The calculated nonrotating frequencies were lower than the measurements (3.3% for the lead-lag mode), which indicates errors in the documented model properties. A similar problem was noted for E927-1; in that case the input properties were adjusted to obtain a match between the calculated and measured nonrotating blade frequencies. However, this was not done for DART, and the calculated regressing lead-lag mode is shifted by approximately 50 rpm from the measurements. The disagreement between the nonrotating frequency measurements and the frequency calculations based on the tabulated mass and stiffness

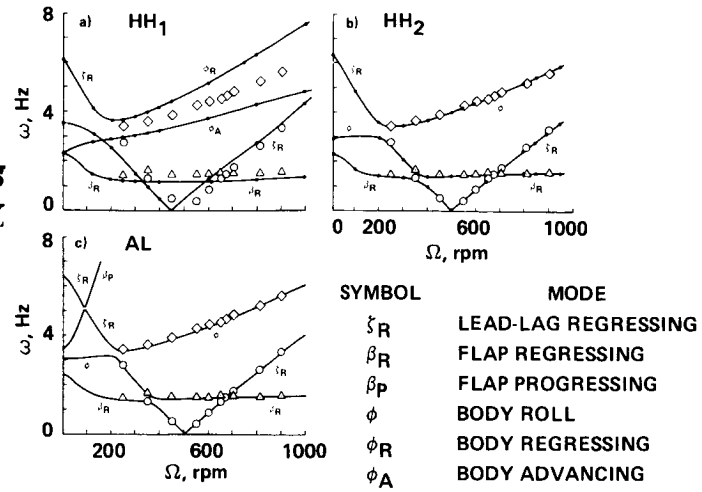

Fig. 3 Individual comparison of theory and experiment for Case 1 for modal frequencies. a) DART, Hughes Helicopters; b) E927-1, Hughes Helicopters; c) FLAIR, Aeromechanics Laboratory.

properties is probably caused by errors in the tabulated properties as these are based on calculations from design drawings rather than measurements.

A second problem with the DART prediction is that this analysis assumes an isotropic support and therefore must calculate two body modes. For a highly anisotropic support as is the case discussed here, one of the modes is an artifact of the modeling assumptions, but there is no way that coupling with this false mode can be avoided. In this case neither mode shows good agreement with the data.

A comparison of the three predictions and the data for the Case 1, regressing-lead-lag-mode damping is shown in Fig. 4. The damping measurements show a weak instability at 675 and 680 rpm which is caused by a coalescence of the regressing lead-lag and flap modes. This weak instability occurs only

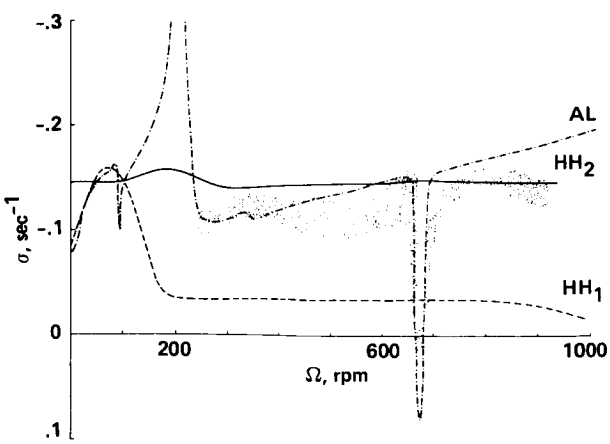

Fig. 4 Composite comparison of theory and experiment for Case 1 for regressing lead-lag mode damping. Data are shown by stippled area; analyses used are DART (HH_1), E927-1 (HH_2), and FLAIR (AL).

for the case of a single-body degree of freedom; with both body pitch and roll freedoms the instability disappears (Ref. 4). The FLAIR calculations, which used a 1- to 2-rpm grid in the vicinity of the instability, show good agreement with the data. Neither the DART nor E927-1 analyses predicted the instability, possibly because neither program calculated damping values for rotor speeds between 650 and 700 rpm.

Both E927-1 and FLAIR show about the same level of damping over most of the rotor speed range. However, DART significantly underpredicts the damping level, which is surprising considering that the damping is largely caused by the rotor structural damping and the profile drag damping.

The three analyses show very different behavior caused by coupling for rotor speeds below 300 rpm. The FLAIR analysis shows a strong effect of coupling of the regressing lead-lag and body roll modes near 200 rpm. The E927-1 program shows significantly less coupling of these two modes, while DART shows no indication of coupling. At about 90 rpm, FLAIR shows similar behavior when the lead-lag regressing and flap-progressing modes couple, but this time DART shows a similar response while E927-1 does not. Acceptable experimental data were not obtained for rotor speeds below 250 rpm so these differences cannot be resolved.

Case 2

Case 2 includes body pitch and roll degrees of freedom; the nonrotating frequencies are nearly identical as shown in Table 2. (Note, however, that the inertias and stiffnesses are not identical.) The fixed-system frequencies for this case are shown in Fig. 5. The behavior in this case is very similar to Case 1 except in Case 2 there are two body modes. At about 875 rpm, the regressing lead-lag and body pitch modes coalesce and a

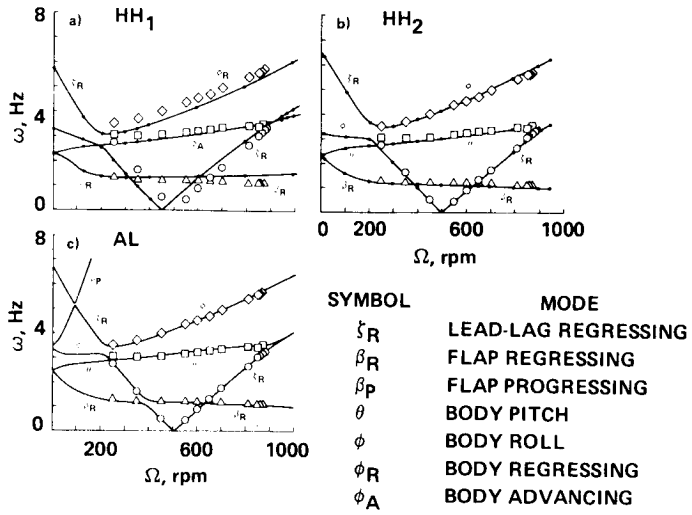

Fig. 5 Individual comparison of theory and experiment for Case 2 for modal frequencies. a) DART, Hughes Helicopters; b) E927-1, Hughes Helicopters; c) FLAIR, Aeromechanics Laboratory.

classical ground-resonance instability occurs. No instability is observed at the regressing lead-lag and flap mode crossing.

The DART analysis shows poor-to-fair correlation for this case, partly because of the frequency shift of the regressing lead-lag mode as discussed previously, and partly because the body regressing mode (body roll mode) frequencies are not well predicted. The E927-1 analysis shows good correlation and FLAIR shows very good predictive capability.

The regressing lead-lag mode damping for Case 2 is shown in Fig. 6. The damping level remains relatively constant until the regressing lead-lag and body pitch mode coalescence where an almost explosive instability occurs--a classic in vacuo ground resonance. The E927-1 and FLAIR analyses both show good to very good agreement with the data, not only in predicting the stability boundary, but also in the level of damping over the entire rotor speed range. As in Case 1 these analyses disagree as to the effect of coupling between the regressing lead-lag and body roll modes in the vicinity of 200 rpm, but no data were obtained that could resolve these differences.

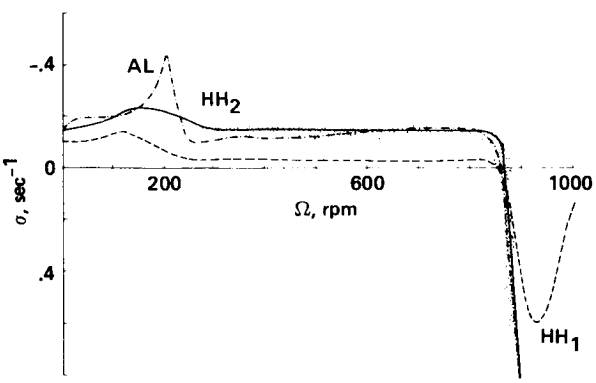

Fig. 6 Composite comparison of theory and experiment for Case 2 for regressing lead-lag mode damping. Data are shown by stippled area; analyses used are DART (HH_1), E927-1 (HH_2), and FLAIR (AL).

The DART predictive capability is fair in this case and the prediction of the neutral stability point is quite good despite the 50-rpm shift. As in Case 1, the reduction in damping away from the instability is puzzling. The damping level predicted between 300 and 800 rpm is significantly less than the structural damping measured at zero rpm.

Conclusions

The DART and E927-1 analyses used by Hughes Helicopters and the U.S. Army Aeromechanics Laboratory FLAIR analysis were compared with two cases from an experiment that measured aeromechanical stability of a model rotor and fuselage in a simulated vacuum. Overall the DART analysis showed poor correlation for this coupled rotor-body data set while the E927-1 predictions were fair-to-good. The FLAIR predictions were judged to be good.

References

[1]Bousman, William G. and Hodges, Dewey H., "An Experimental Study of Coupled Rotor-Body Aeromechanical Instability of Hingeless Rotors in Hover," Vertica, Vol. 3, 1979, pp. 221-244.

[2]Bousman, William G., "An Analog Technique for the Measurement of Damping from Transient Decay Signals," NASA TM X-73,121, June 1976.

[3]Bousman, William G., "An Experimental Investigation of Hingeless Helicopter Rotor-Body Stability in Hover," NASA TM-78489, June 1978.

[4]Ormiston, Robert A., "Aeromechanical Stability of Soft Inplane Hingeless Rotor Helicopters," Paper No. 25, Third European Rotorcraft and Powered Lift Aircraft Forum, Aix-en-Provence, France, Sept. 1977.

Appendix A--Model Properties

The two cases examined in this paper are from an experiment originally reported in Ref. 3. The experimental model properties in this appendix are taken from that reference with the exception of the tabulated mass and stiffness properties in Tables 4-7, which have not been reported before. In addition, a few errors have been found in the Ref. 3 documentation, so these are noted.

Rotor Properties

The major rotor geometric properties have been tabulated in Table 1. Additional descriptive properties are shown in Table 3. The profile drag coefficient is assumed to be approximately 1.0 based on a Reynolds number of 10,000 to 35,000 at the three-quarter span.

Table 3 Rotor Descriptive Properties

Property	Value
Blade number, b	3
Airfoil section	circular
Lift curve slope, a	0.0
Profile drag coefficient, c_{d_o}	1.0
Height above gimbal axes, h, cm	24.1

The design drawings of the hub and tantalum blade were used to calculate mass, stiffness, and pitching inertias outboard of blade station 2.034 in. This blade station is the outer face of the leftmost part in the exploded drawing of Fig. 2. Properties are tabulated separately for the lead-lag flexure, side beams, and flap flexure in Tables 4 to 6. Table 7 provides the composite properties for these components outboard of B.S. 2.034 in. Running weight and pitch inertia were assumed additive in this table and the combined stiffness was based on a series-spring representation. The calculated properties outboard of the flap flexure for B.S. 4.423 in. are also included in this table.

Measurements were made of the mass, mass centroid, and moment of inertia of one flap flexure/combination, as shown in Table 8. These measurements were adjusted to correct for the effect of that portion of the flap flexure inboard of the flap flexure centerline (B.S. 3.35 in.) and to add the contribution of the lead-lag flexure and side beams. The mass properties of the blade and hub outboard of the flap flexure centerline, shown in Table 8, were calculated from Table 7. These compare quite well with the measurements for mass and centroid, but are 3.5% too high for the flapping inertia. No measurements were made of pitch inertia or rotor polar inertia. Note that the values shown in Table 4 of Ref. 3 are in error for pitch inertia and rotor polar inertia.

The first flap- and lead-lag mode frequency and damping were measured as installed on the model with the body degrees of freedom locked out. The measured frequency values, shown in Table 9, are compared to calculated values based on

$$\omega = \sqrt{K/I_o}$$

where the stiffness is assumed to be due solely to the flexures

$$K = \frac{EI}{\ell}$$

and the EI and ℓ values are from Table 7 for B.S. 3.111 to 3.588 in. for the flap flexure and B.S. 3.225 to 3.450 in. for the lead-lag flexure. The blade inertia, I_o, is the value calculated in Table 8. As the calculated inertia was 3.5% higher than the measured value, it is expected that the calculated frequencies should be 1.7% low. As is shown in Table 9, the calculated flap frequency is 1.0% high and the lead-lag frequency is 5.5% low. The stiffnesses of the flexures are very sensitive to the thickness. The thickness specified on the design drawing of the lead-lag flexure is 0.0250 ±0.0005 in. If the frequency is calculated with the flexure assumed to be 0.0255 in. thick, then the value is 6.23 Hz which is 2.7% low. The sensitivity of the frequency to flexure dimensional data suggests that the EI values should be adjusted to match the nonrotating frequency data which represent an accurate experimental measurement. The nonrotating lead-lag damping measured on the model was 0.185% critical.

Body Properties

The body was weighed without the gimbal frame or hub hardware. The weight of the hub hardware inboard of the flap flexure centerline was added to the measured weight to give a value of the body mass of 42.48 lb_m. The center of gravity of the body mass was not determined, but was assumed coincident with the gimbal center.

The body pitch and roll inertias were determined for the Case-2 configuration by measuring the gimbal spring stiffnesses and the body frequencies with the rotor hardware removed. The inertias were calculated assuming a single-degree-of-freedom

Table 4 Calculated Mass and Stiffness Properties of Lead-Lag Flexure[a]

BLADE STATION in.	WEIGHT lb_m/in.	EI_f 10^6 lb-in^2	EI_c 10^6 lb-in^2	GJ 10^6 lb-in^2	I_θ lb_m-in^2/in.
2.431	0.422	5.18	5.18	3.93	0.101
2.581	0.422	5.18	5.18	3.93	0.101
2.581	0.0682	1.11	0.179	0.116	0.0110
2.750	0.0682	1.11	0.179	0.116	0.0110
2.791	0.0398	0.756	0.0102	0.116	0.0110
2.890	0.0266	0.597	0.00701	0.116	0.0110
2.989	0.0398	0.756	0.0102	0.116	0.0110
3.030	0.0682	1.11	0.0179	0.116	0.0110
3.200	0.0682	1.11	0.0179	0.116	0.0110
3.200	0.0292	0.477	0.00141	0.00139	0.00155
3.225	0.0097	0.159	0.0000521	0.00139	0.00155
3.450	0.0097	0.159	0.0000521	0.00139	0.00155
3.475	0.0292	0.477	0.00141	0.00139	0.00155
3.475	0.0682	1.11	0.0179	0.114	0.0110
3.553	0.0682	1.11	0.0179	0.114	0.0110
3.585	0.0451	0.857	0.0118	0.114	0.0110
3.663	0.0357	0.745	0.00935	0.114	0.0110
3.741	0.0451	0.857	0.0118	0.114	0.0110
3.773	0.0682	1.11	0.0179	0.114	0.0110
4.101	0.0682	1.11	0.0179	0.114	0.0110

a MAT'L – 17-4 PH STAINLESS; ρ = 0.282 lb_m/in^3, E = 29 × 10^6 lb/in^2, G = 11 × 10^6 lb/in^2.
b AXIS OF SYMMETRY COINCIDENT WITH 0.25c

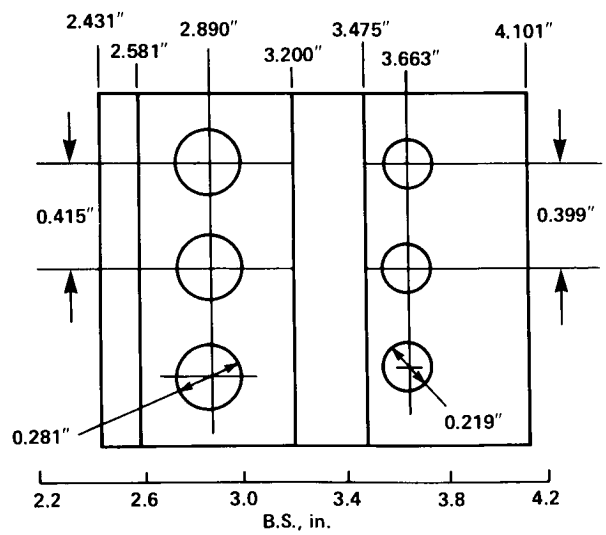

LEAD-LAG FLEXURE

Table 5 Calculated Mass and Stiffness Properties of Side Beams[a]

BLADE STATION in.	WEIGHT lb_m/in.	EI_f 10^6 lb-in^2	EI_c 10^6 lb-in^2	GJ 10^6 lb-in^2	I_θ lb_m in^2/in.
2.633	0.0535	0.468	0.298	0.0109	0.0105
2.883	0.0535	0.468	0.298	0.0109	0.0105
2.883	0.0410	0.359	0.190	0.0109	0.00493
2.983	0.0410	0.359	0.190	0.0109	0.00493
3.029	0.0234	0.269	0.109	0.0109	0.00493
3.139	0.0160	0.221	0.0745	0.0109	0.00493
3.249	0.0234	0.269	0.109	0.0109	0.00493
3.295	0.0410	0.359	0.190	0.0109	0.00493
3.439	0.0410	0.359	0.190	0.0109	0.00493
3.485	0.0234	0.269	0.109	0.0109	0.00493
3.595	0.0160	0.221	0.0745	0.0109	0.00493
3.705	0.0234	0.269	0.109	0.0109	0.00493
3.751	0.0410	0.359	0.190	0.0109	0.00493
3.851	0.0410	0.359	0.190	0.0109	0.00493
3.851	0.0613	0.537	0.220	0.0109	0.00957
4.101	0.0613	0.537	0.220	0.0109	0.00957

a MAT'L – Ti-6Al-4V ALLOY; $\rho = 0.160$ lb_m/in^3, $E = 16 \times 10^6$ lb/in^2, $G = 6.2 \times 10^6$ lb/in^2.

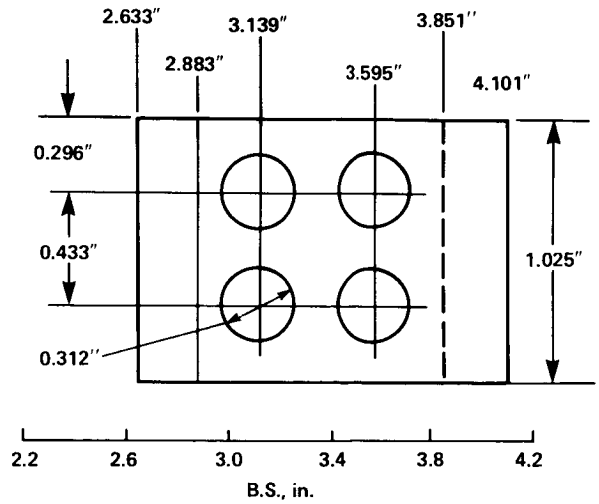

SIDE BEAMS

Table 6 Calculated Mass and Stiffness Properties of Flap Flexure[a]

BLADE STATION in.	WEIGHT lb_m/in.	EI_f 10^6 lb-in^2	EI_c 10^6 lb-in^2	GJ 10^6 lb-in^2	I_θ lb_m in^2/in.
2.633	0.276	2.49	9.20	9.92	0.114
2.883	0.276	2.49	9.20	9.92	0.114
2.883	0.0510	0.0156	1.70	1.46	0.0167
3.088	0.0510	0.0156	1.70	1.46	0.0167
3.088	0.0186	0.000759	0.621	0.0192	0.00106
3.111	0.0062	0.000028	0.207	0.0192	0.00106
3.588	0.0062	0.000028	0.207	0.0192	0.00106
3.611	0.0186	0.000759	0.621	0.0192	0.00106
3.611	0.510	0.0156	1.70	0.185	0.0167
4.223	0.510	0.0156	1.70	0.185	0.0167
4.223	0.242	2.00	0.763	3.98	0.0839
4.298	0.242	2.00	0.763	3.98	0.0839
4.298	0.368	3.54	6.62	3.98	0.0988
4.423	0.368	3.54	6.62	3.98	0.0988

a MAT'L – 17-4 PH STAINLESS; ρ = 0.282 lb_m/in^3, E = 29 × 10^6 lb/in^2, G = 11 × 10^6 lb/in^2. AXIS OF SYMMETRY COINCIDENT WITH 0.25c.

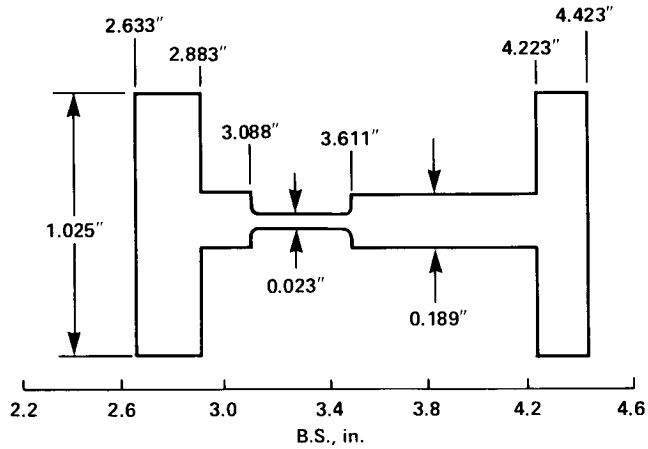

FLAP FLEXURE

Table 7 Calculated Mass and Stiffness Properties of Hub Flexure and Tantalum Blade

Blade station, in.	Weight, lb_m/in.	EI_f, 10^6 lb-in.^{2}	EI_c, 10^6 lb-in.^{2}	GJ, 10^6 lb-in.^{2}	I_θ, lb_m in.^{2}/in.
2.034	0.573	20.1	20.1	15.6	0.403
2.431	0.573	20.1	20.1	15.6	0.403
2.431	0.422	5.18	5.18	3.93	0.101
2.581	0.422	5.18	5.18	3.93	0.101
2.581	0.0533	1.11	0.0179	3.93	0.101
2.633	0.0533	1.11	0.0179	3.93	0.101
2.633	0.398	0.291	0.0169	0.00995	0.136
2.750	0.398	0.291	0.0169	0.00995	0.136
2.791	0.369	0.259	0.00985	0.00995	0.136
2.883	0.357	0.239	0.00706	0.00995	0.136
2.883	0.120	0.0146	0.00695	0.00990	0.0326
2.890	0.119	0.0146	0.00673	0.00990	0.0326
2.983	0.131	0.0147	0.00945	0.00990	0.0326
2.989	0.131	0.0147	0.00962	0.00990	0.0326
3.030	0.143	0.0146	0.0152	0.00990	0.0326
3.088	0.139	0.0145	0.0148	0.00990	0.0326
3.088	0.106	0.000756	0.0146	0.00656	0.0170
3.111	0.0923	0.000028	0.0138	0.00656	0.0170
3.139	0.0904	0.000028	0.0135	0.00656	0.0170
3.200	0.0945	0.000028	0.0140	0.00656	0.0170
3.200	0.0555	0.000028	0.00138	0.00116	0.00754
3.225	0.0377	0.000028	0.000052	0.00116	0.00754
3.249	0.0393	0.000028	0.000052	0.00116	0.00754
3.295	0.0569	0.000028	0.000052	0.00116	0.00754
3.439	0.0569	0.000028	0.000052	0.00116	0.00754
3.450	0.0527	0.000028	0.000052	0.00116	0.00754
3.475	0.0626	0.000028	0.00139	0.00116	0.00754
3.475	0.102	0.000028	0.0146	0.00655	0.0170
3.485	0.0978	0.000028	0.0143	0.00655	0.0170
3.553	0.0932	0.000028	0.0142	0.00655	0.0170
3.585	0.0680	0.000028	0.00976	0.00655	0.0170
3.588	0.0674	0.000028	0.00968	0.00655	0.0170
3.595	0.0699	0.000250	0.00967	0.00655	0.0170
3.611	0.0777	0.000756	0.00952	0.00655	0.0170
3.611	0.110	0.0143	0.00961	0.00944	0.0326
3.663	0.107	0.0144	0.00848	0.00944	0.0326
3.705	0.115	0.0145	0.00969	0.00944	0.0326
3.741	0.133	0.0146	0.0110	0.00944	0.0326
3.751	0.144	0.0147	0.0127	0.00944	0.0326
3.773	0.160	0.0148	0.0162	0.00944	0.0326
3.851	0.160	0.0148	0.0162	0.00944	0.0326
3.851	0.181	0.0150	0.0164	0.00944	0.0373
4.101	0.181	0.0150	0.0164	0.00944	0.0373
4.101	0.051	0.0156	1.70	0.185	0.0167
4.223	0.051	0.0156	1.70	0.185	0.0167
4.223	0.242	2.00	0.763	3.98	0.0839
4.298	0.242	2.00	0.763	3.98	0.0839
4.298	0.368	3.54	6.62	3.98	0.0988
4.423	0.368	3.54	6.62	3.98	0.0988
4.423	0.615	9.18	9.18	6.74	0.175
4.573	0.615	9.18	9.18	6.74	0.175
4.573	0.222	0.761	0.761	0.558	0.0163
5.423	0.222	0.761	0.761	0.558	0.0163
5.423	0.118	0.0921	0.0921	0.0676	0.00369
14.963	0.118	0.0921	0.0921	0.0676	0.00369

Table 8 Hub and Blade Mass Properties

Quantity	Measured	Adjusted[a]	Calculated	Error[b]
Mass, lb_m	1.582	1.570	1.574	+0.3%
Centroid of mass with respect to center, in.	8.455	8.594	8.580	-0.2%
Flapping and lead-lag inertia, lb_m-in.^{2c}	60.48	59.87	61.99	+3.5%
Pitch inertia, lb_m-in.^{2}	--	--	0.116	--
Rotor polar inertia, lb-in.^{2}	--	--	414.0	--

[a]Flap flexure effect inboard of B.S. 3.35 not included (Table 6); effect of lead-lag flexure (Table 4) and side beams (Table 5) included.
[b]Based on adjusted measurement.
[c]With respect to B.S. 3.35 in.

Table 9 Rotor Modal Frequency

Modal Frequency, Hz	Measured	Calculated	Error
Flap	3.01[a]	3.04	+1.0%
Lead-lag	6.39	6.04	-5.5%

[a]Not measured directly because of flap stop restraint. Obtained from ratio of measurements made with a conventional blade installed.

oscillator and were then corrected to add the inertia of the rotor hardware inboard of the flap-flexure centerline. The measured stiffnesses and calculated inertias are shown in Table 10. The correction to the inertia for the rotor hardware is considered more accurate than the values of Ref. 3. If the rotor inertia is added to the body inertias, then uncoupled, nonrotating body frequencies can be calculated and compared to the measured coupled, nonrotating body frequencies from Table 2. Large differences between the coupled and uncoupled frequencies are not expected because the flap degree of freedom is restrained by a droop stop, and the lead-lag frequency is well separated in frequency. The calculated pitch and roll frequencies are respectively -1.6 and 5.5% apart from the measurements which suggests the inertia properties are reasonably correct.

The body damping is highly nonlinear (see Ref. 3 for a detailed discussion). Representative values of body damping of 3% have been assumed in pitch and roll.

Appendix B--Experimental Data

Tables 11 and 12 show the measured rotor speed, modal frequencies, and regressing lead-lag damping for Cases 1 and 2. These data were obtained in the experiment reported in Ref. 3. The various modes were individually excited and the modal frequency and damping were obtained from the transient decay using an analog technique described in Ref. 2. Modal damping of the body pitch and roll modes was not obtained because of nonlinear damping in the gimbal bearings. Except as noted, the regressing lead-lag mode damping was linear.

Appendix C--Correlation

All of the theoretical predictions and experimental data for the selected cases are shown in this appendix in Figs. 7-12. In some cases figures

Table 10 Body Properties

Quantity	Body Pitch	Body Roll
Gimbal stiffness, in.-lb/rad	1480	849
Inertia about gimbal, lb_m-in.^{2}	1710	603
Uncoupled body frequency, Hz[a]	2.54	2.69
Coupled body frequency, Hz[b]	2.58	2.55

[a]Includes 543 lb_m-in.^{2} for rotor inertia.
[b]From Table 2.

from the main text are repeated here for completeness. Two formats are used for the correlation. The first format compares the theoretical predictions and experimental data individually for each mathematical model used. The second format compares all the theoretical predictions on a single composite plot and the experimental data are shown as a stippled area. An exception to this format is that no composite comparison is made of modal frequencies. A code is used to identify the theoretical predictions for both the individual and composite comparisons; it is explained in Table 13.

Table 11 Modal Frequencies and Damping, Case 1

Rotor Speed, rpm	Regressing Flap Frequency, Hz	Body Roll Frequency, Hz	Regressing Lead-lag Frequency, Hz	Regressing Lead-lag Damping, sec^{-1}
250	1.44	3.44	2.75	-0.104
	1.45	--	2.75	-0.098
	1.50	--	2.77	-0.114
350	1.36	3.76	1.66	-0.115
	1.30	3.61	1.66	-0.118
	1.32	3.65	1.67	-0.131
450	1.52	3.92	0.52	-0.112
	1.44	3.92	0.52	-0.130
	1.44	3.91	0.51	-0.101
550	1.52	4.40	0.44	-0.096
	1.48	4.24	0.43	-0.114
	1.46	4.27	0.44	-0.115
	1.52	4.23	0.45	-0.111
	1.51	4.24	0.46	-0.104
	--	--	0.45	-0.117
600	1.52	4.41	0.89	-0.119
	1.46	4.48	0.90	-0.121
	1.45	4.41	0.89	-0.105
	--	4.41	0.89	-0.136
	--	4.43	0.89	-0.133
	--	4.40	--	--
	--	4.58	--	--
	--	4.58	--	--
650	1.59	4.62	1.34	-0.112
	1.57	4.60	1.35	-0.114
	--	4.58	1.35	-0.143
	--	4.61	1.35	-0.155
	--	4.62	1.34	-0.156
670	--	--	1.51	0.010
	--	--	1.51	0.005
	--	--	1.51	0.003
675	1.53	4.64	1.54	-0.013
	1.52	4.80	1.54	-0.015
	--	4.71	1.55	-0.013
	--	4.71	--	--
705	1.60	4.96	1.78	-0.120
	1.55	4.81	1.78	-0.130
	1.54	4.82	1.81	--
810	1.52	5.28	2.65	-0.159
	1.54	5.26	2.64	-0.150
	1.55	5.24	2.64	-0.140
900	1.60	5.68	3.35	-0.147
	1.57	5.65	3.34	-0.136
	1.58	5.63	3.35	-0.128

Table 12 Modal Frequencies and Damping, Case 2

Rotor Speed, rpm	Regressing Flap Frequency, Hz	Body Pitch Frequency, Hz	Body Roll Frequency, Hz	Regressing Lead-lag Frequency, Hz	Regressing Lead-lag Damping, Hz
250	1.34	3.07	3.52	2.77	-0.107
	1.32	3.04	--	2.77	-0.115
	1.28	--	--	2.77	-0.109
350	1.22	3.02	3.69	1.64	-0.125
	1.22	3.06	3.68	1.65	-0.161
	1.20	2.96	3.68	1.63	-0.130
450	1.24	3.06	3.99	0.53	-0.161
	1.24	3.07	3.93	0.52	-0.133
	1.20	3.04	4.00	0.53	-0.123
550	1.20	3.15	4.32	0.43	-0.133
	1.22	3.16	4.33	0.43	-0.139
	1.20	3.12	4.40	0.42	-0.133
600	1.20	3.19	4.52	0.88	-0.150
	1.19	3.24	4.53	0.88	-0.129
	1.20	3.20	4.56	0.88	-0.134
650	1.20	3.29	4.70	1.32	--
	1.20	3.28	4.71	1.32	--
	1.20	3.28	4.72	1.31	--
700	1.19	3.33	4.93	1.76	-0.123
	1.17	3.35	4.95	1.77	-0.155
	1.20	3.36	4.96	1.76	-0.140
810	1.13	3.45	5.40	2.68	-0.134
	1.12	3.43	5.39	2.68	-0.143
	1.12	3.44	5.40	2.70	-0.140
	--	--	--	2.68	-0.160
	--	--	--	2.68	-0.167
	--	--	--	2.69	-0.156
850	1.11	3.36	5.56	3.05	-0.097
	1.10	3.35	5.56	3.04	-0.112
	1.12	3.44	5.60	3.03	-0.103
860	1.10	3.32	5.58	3.15	-0.090
	1.10	3.30	5.62	3.17	-0.031
	--	--	--	3.14	-0.064
870	1.12	3.37	5.68	3.25	-0.022
	1.11	3.38	5.70	3.27	-0.034-0.265[a]
	1.09	3.40	5.70	3.25	-0.126[a]
880	--	--	--	3.35	0.570
	--	--	--	3.37	0.395-0.632[a]
	--	--	--	3.34	0.603

[a]Apparent nonlinearity.

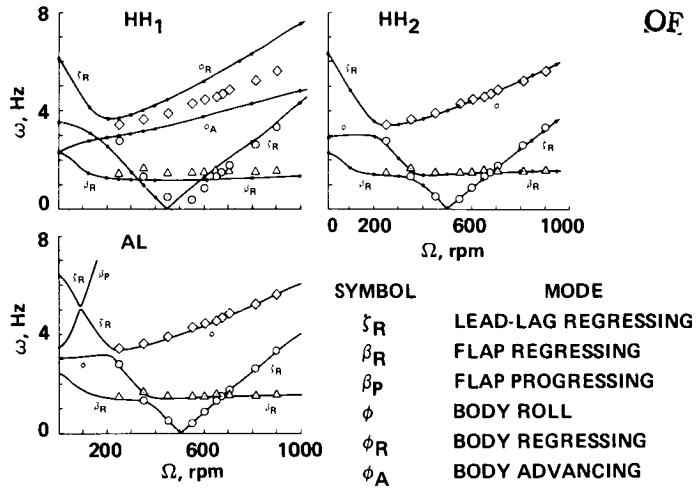

Fig. 7 Individual comparison for Case 1 modal frequencies.

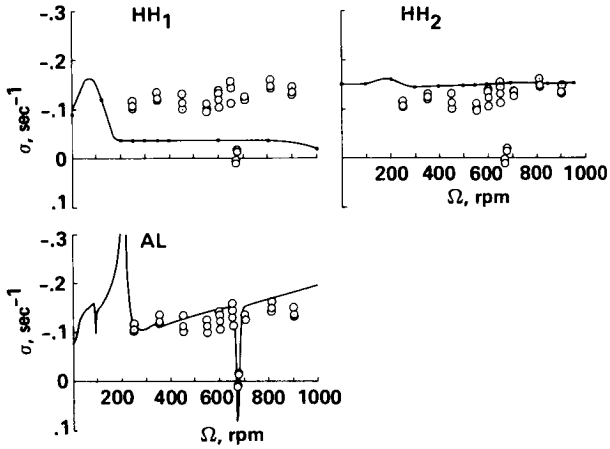

Fig. 8 Individual comparison for Case 1 regressing lead-lag mode damping.

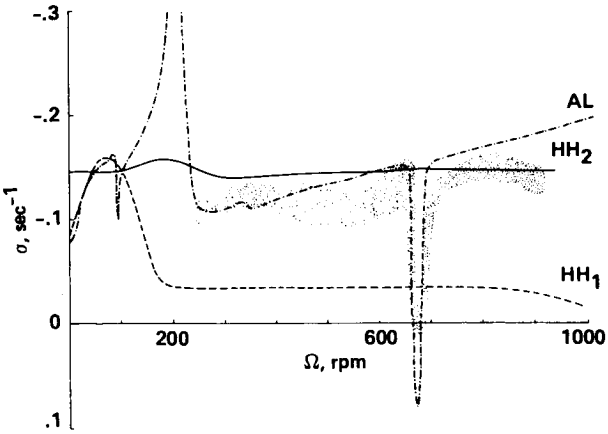

Fig. 9 Composite comparison for Case 1 regressing lead-lag mode damping.

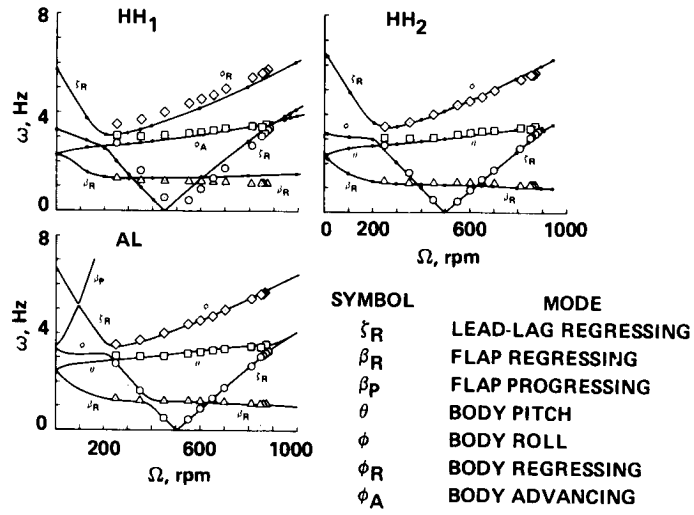

Fig. 10 Individual comparison for Case 2 modal frequencies.

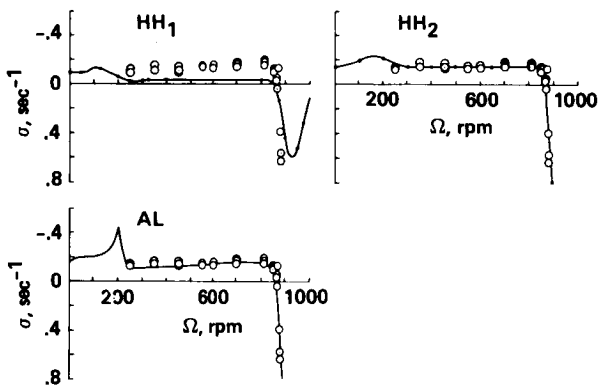

Fig. 11 Individual comparison for Case 2 regressing lead-lag mode damping.

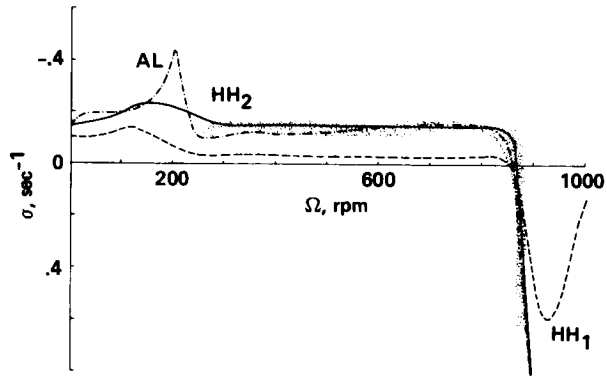

Fig. 12 Composite comparison for Case 2 regressing lead-lag mode damping.

Table 13 Explanation of Prediction Codes

Code	Prediction Method	User
HH_1	DART	Hughes Helicopters
HH_2	E927-1	Hughes Helicopters
AL	FLAIR	U.S. Army Aeromechanics Laboratory